Tumor-microenvironment Responsive Targeted Exosome-like Nanovesicles From Dunaliella Salina for Enhancing Gene/immune Combination Therapy

Mengxi Zhu
Henan University of Science and Technology
Shan Li
Henan University of Science and Technology
Shuying Feng
Henan University of Traditional Chinese Medicine
Haojie Wang
Henan University of Science and Technology
Lina Hu
Henan University of Science and Technology
Shegan Gao
Henan University of Science and Technology
Yingjie Yu
Henan University of Science and Technology
Gaofeng Liang (lgfeng990448@163.com)
Henan University of Science and Technology https://orcid.org/0000-0003-0097-0296

Research Article

Keywords: exosome-like nanovesicles, Dunaliella salina, anti-PD-L1, miR-375, esophageal cancer, co-delivery

Posted Date: August 6th, 2021

DOI: https://doi.org/10.21203/rs.3.rs-733290/v1

Abstract

Background

As an endogenous extracellular vesicle, exosome is increasingly presenting its great potential in the field of drug delivery. However, it is the bottleneck to obtain a large number of uniform, stable and multi-component controllable exosomes with low cost and time.

Results

In this study, we develop a novel targeted drug delivery system based on exosome-like nanovesicle by use of natural marine single-celled *Dunaliella salina* (DENV), the c(RGDyK) peptide has been conjugated to DENV surface to achieve the targeted delivery to esophageal cancer cells. Furthermore, miR-375 has been loaded into the cRGD-DENV through electroporation, and aPD-L1 has been conjugated onto its surface via Gly-PLGLAG-Cys peptide, a matrix metalloproteinase-2 (MMP-2)-cleavable peptide, which facilitates the release of aPD-L1 in tumor environment to achieve the high-efficiency combination of gene therapy and immunotherapy. Firstly, the engineered DENV delivery system was prepared and characterized. It exhibited a proper particle diameter (approximately 150 nm) with in vitro sustained release features in the presence of MMP-2/9. More importantly, the cRGD-DENV was effective, promoted selective delivery of cargo to the target site, and reduced nonspecific uptake, consequently, significantly inhibit tumor growth *in vitro* and *in vivo*.

Conclusion

The specific nanocarrier delivery system provide a promising strategy for the rapid and large-scale production of functionalized exosome-like nanovesicle by adapting multifunctional peptides specifically targeted tumor.

Background

Exosomes, also called “Trojan-Horse”, are naturally transported small membrane vesicles (30-150 nm) of endocytosis origin, have been used for facilitating intracellular delivery of numerous diverse cargoes [1, 2], and are closely related to many physiological or pathological processes[3, 4]. In recent years, the plethora of peer-reviewed publications and the explosion of new exosome-based biotechnology companies focused on modifying and exploiting exosomes as biomarkers, vaccine/drug carriers, or novel therapeutics demonstrates the great interest of many researchers in this field. Especially, exosomes are increasingly presenting its great potential in the field of drug delivery due to its nano-scale size, low immunogenicity and low toxicity [5-7]. For example, mammalian cell-derived exosomes can be used as drug delivery vehicles to encapsulate drugs (DOX, paclitaxel, curcumin) for tumor treatment[8], however, exosome derived from mammalian cell are limited in clinical application due to the high cost for mass production, time-consuming, and uncontrolled contents[9]. Therefore, it is urgent to develop safe alternative sources of exosome to solve the problem that limits its further application.

Recently, exosome-like nanovesicles derived from plants have attracted much attention due to the merits of high yields, low production costs and low cytotoxicity [9, 10]. Inspired by this, *Dunaliella salina* (*D. salina*), a single-celled halophilic eukaryotic algae without cell walls, was selected to prepare exosome-like nanovesicles. As a photosynthetically autotrophic organism, *D. salina* grows fast, easy to cultivate, rich in essential glycerol and β-carotene[11, 12]. More importantly, *D. salina* can be grown on a large scale in seawater, which determines that we can obtain exosome-like nanovesicles at lower cost and shorter production times compared with mammalian cells. Therefore, *D. salina* can be used as a promising bioreactor to produce large amounts of exosome-like nanovesicles for targeted drug delivery.

In this study, we innovatively used natural single-cell *D. salina* for the preparation of exosome-like nanovesicles (DENV). To improve its targeting capability, the c(RGDyK) (cyclo(Arg-Gly-Asp-D-Tyr-Lys) peptide, a specific tumor-homing polypeptides, was conjugated on DENV surface to construct engineered exosomes (cRGD-DENV) in order to facilitate targeting cellular uptake through $\alpha_v\beta_3$ integrin receptor-mediated endocytosis in tumor cells and tissue[13-15]. Ultracentrifugation was used to obtain a large number of exosome-like nanovesicles and transmission electron microscope (TEM) was used to characterize them. Then we proved that cRGD-DENV can be specifically taken up by tumor cells, and near-infrared fluorescence (NIRF) imaging indicated that the cRGD-DENV could target to tumor site after intravenous injection, suggesting cRGD-modified DENV could be a promising nano-platform for tumor-targeted therapy. Furthermore, miR-375 was loaded into the cRGD-DENV by electroporation, and the Gly-PLGLAG-Cys peptide (a MMP-2 sensitive peptide), which can be cleaved by the highly expressed MMP-2 in the tumor microenvironment (TME) [16, 17], was used as linker between aPD-L1 and DENV. The schematic of targeted drug delivery system based on DENV was shown in Fig. 1. In this design, the delivery system can achieve the purpose of releasing aPD-L1 and miR-375 sequentially: the high expression of matrix metalloproteinase in TME can cleave the Gly-PLGLAG-Cys peptide, and the aPD-L1 was released from cRGD-DENV-aPD-L1/miR-375 when this delivery system enter into tumor surroundings. Subsequently, the released aPD-L1 binds to the PD-L1 on tumor cells to enhance antitumor immune response of the immune system, and then miR-375 was delivered into tumor cells, and played a post-transcriptional regulatory role in cells. Moreover, we investigated the physiological role of engineered DENV derived from *D. salina* in esophageal cancer cells and the capability of drug delivery *in vivo*. The results of this study provide strong evidence that exosome-like nanovesicles derived from *D. salina* are novel delivery biomaterials with extensive broad clinical application potential.

Results And Discussion

Characterization of DENV-based delivery system

As a nanoscale membrane vehicle, exosomes are believed to be a promising carrier being their unique properties, including low immunogenicity, biodegradability, low toxicity, effective protection for cargoes and even cross the BBB [18-21]. However, how to obtain large quantities of exosomes with lower cost and time-consuming remains a challenge. Recently, exosome-like nanovesicles from microbial and plant to

human cells were investigated, and plant-derived nanovesicles have been gained widespread attention due to their low toxicity, easy availability, anti-cancer potential and anti-inflammatory activities[10, 22-24]. In this study, *D. salina,* a single-celled halophilic eukaryotic algae [25, 26], being photosynthetically autotrophic and having the advantages of rapid growth, less biological toxicity, rich in glycerol and β-carotene, was used as source of exosome-like nanovesicles with high yield and purity[27]. DENV was isolated from the supernatant of *D. salina* by multistep differential centrifugation, and BCA protein assay was used to determine the protein concentration of the DENV. According to the results, 100 μg DENV could be extracted per 100 mL culture supernatant, and the concentration required for the experiment can be obtained by multiple extractions.

To achieve tumor targeting *in vivo*, targeting ligands (such as antibodies and polypeptides) were conjugated to exosomal surface to enhance specific interactions between exosomes and target cells [28, 29]. For instance, the RVG peptide, a rabies virus glycoprotein, was conjugated to the exosomal surface (RVG-Exo), and the results showed the RVG-Exo could target the lesion region of the ischemic brain after intravenous administration[30]. Furthermore, Kim G et al modified exosomes with T7 peptides (T7-Exo), which were transferrin receptor-binding peptides, and found T7-Exo had higher delivery efficiency to C6 glioblastoma cells compared with RVG-Exo[31]. The c(RGDyK) peptide, exhibiting high affinity to integrin $\alpha_v\beta_3$, is highly expressed in most tumors, such as esophageal cancer, glioma, breast cancer[32-34]. Here, the cRGD peptide was modified on the DENV by chemical coupling. Firstly, DENV was labeled with DIO, cRGD was labeled with Cy5.5-NHS, and consequences were recorded under a confocal laser scanmicroscope (CLSM) (Fig. 2A-C). The result of fluorescence co-localization indicated that green fluorescence overlaps with red fluorescence and a yellow fluorescence bright spot appeared, indicating that a successful coupling of DENV and cRGD peptide.

Then TEM was used to identify the morphology of engineered DENV, as shown in Fig. 2D-E. DENV presented a typical "disc" shape with an average diameter of about 100 nm (Fig. 2D-a1), which was analogous with the reported exosomal size in animal cells[35, 36]. Then, DENV size was analyzed using a dynamic light scattering particle size analyzer (DLS). And the particle size distribution of DENV in aqueous solution was mainly concentrated at 106 nm (Fig. 2D-b1), which was roughly consistent with the results observed under TEM. After modification with miR-375 and aPD-L1, the size was increased to around 150 nm (Fig. 2E-a2and 2E-b2), slightly larger than DENV. Next, we detected the Zeta potential value. As shown in Fig. 2D-c1, the Zeta potential of DENV was about -5.76 mV, however, after loading miR-375 and aPD-L1, and the Zeta potential was shown to be approximately -26.2 mV (Fig. 2E-c2), which revealed that the loading of negatively charged miR-375 increased the negative charge. These results are constant with the characterization of typical exosomes, confirming successful separation of DENV and formulation preparation of cRGD-DENV-aPD-L1/miR-375.

Cell uptake of DENV-based delivery system

To explore the dynamics of the internalization of DENV modified with cRGD polypeptide in KYSE-150 cells, laser confocal microscope fluorescence images of KYSE-150 cells were recorded at 1, 3, 6, and 12 h after incubating DIO-labeled DENV (DIO-DENV, 0.5mg/mL). Fig. 3 showed the series images of DIO-DENV entering esophageal cancer cells. Analysis of the images showed the intensity of green fluorescence in KYSE-150 cells increased up to the 6 h time point and thereafter decreased in 12 h; its intensity of green fluorescence was about one-fifth of that of the 6 h time point. The decrease of DIO fluorescence may result from processing of internalized DENV by KYSE-150 cells, and/or fluorescence quenching of the DIO molecules. Remarkably, cRGD-DENV (right) were internalized more by KYSE-150 cells in contrast to DENV (left), which showed that cRGD modification can enhance significantly the internalization of DENV in KYSE-150 cells, further indicating that better targeting properties of RGD-DENV can be achieved *in vivo*.

Release of aPD-L1 *in vitro*

To achieve TME-triggered rapid release of aPD-L1 in tumor tissues. Gly-PLGLAG-Cys, a substrate peptide sensitive enough to MMPs, highly expressing in a wide range of cancer types [37], were selected as a liker between DENV and aPD-L1. Firstly, we studied the release of aPD-L1 from cRGD-DENV-aPD-L1/miR-375. As shown in Fig. 4A, aPD-L1 conjugated on surface of cRGD-DENV-aPD-L1/miR-375 was almost completely released within 8 h in PBS containing MMPs, in contrast, only a few aPD-L1 was released in the medium of PBS without MMPs. In addition, there was little effect on the release of aPD-L1 from cRGD-DENV-aPD-L1/miR-375 pH of 7.4 and 6.5 *in vitro* (Fig. 4B). These results indicated that cRGD-DENV-aPD-L1/miR-375 was highly sensitive to MMPs, and rapid release of aPD-L1 in the presence of MMPs.

Next, the sensitivity of Gly-PLGLAG-Cys to MMPs was further investigated by cellular uptake assay. As shown in Fig. 5, aPD-L1 was rapid released from cRGD-DENV-aPD-L1/miR-375 in 2 h and most Cy5.5-labeled aPD-L1 (red) didn't obviously increase with time in the presence of MMPs. aPD-L1 colonized surroundingly the cell membrane, indicating that Gly-PLGLAG-Cys could be cleaved by MMPs in TME when cRGD-DENV-aPD-L1/miR-375 delivery system reached the tumor site, which was consistent with the results of release assay *in vitro*. Furthermore, we found that DENV carried miR-375 (green) entered into the cytoplasm after aPD-L1 was released. These results indicated that the DENV delivery system could effectively target to tumor cells and realized drug release sequentially in tumor environment.

Inhibition of cell proliferation, migration and invasion

Then cRGD-DENV loaded with miR-375 and aPD-L1 was used to investigate the effects of proliferation, migration and invasion on esophageal cancer cells *in vitro*. As shown in Fig. 6A, cRGD-DENV-aPD-L1/miR-375 group showed a significantly inhibition than the other treatment groups alone, indicating that the combination of aPD-L1 and miR-375 had the optimal suppression effect on KYSE-150 cells. Moreover, we used the wound-healing and Transwell experiment to study the migration and invasion of the delivery system on KYSE-150 cells. In Fig. 6B-C, after 72 h, the wound-like gaps in the untreated and DENV-treated cells had healed almost completely, while cRGD-DENV-aPD-L1/miR-375 group still a large gap. Fig. 6D

exhibited a cell invasion with similar inhibition results as cell migration in the effects of different treatments group. Taken together, the cRGD-DENV-aPD-L1/miR-375 group demonstrated a notable inhibitory effect on migration and invasion of KYSE-150 cells.

Flow cytometry assay and gene expression monitoring

Next, we investigated the effect on KYSE-150 cells of the engineered DENV. Flow cytometry were used to detect cellular apoptosis rate after treatment with different formulations for 48 h. As shown in Fig. 7A, the early apoptosis rate of KYSE-150 cells with different treatments were about 1.02% (untreated), 3.08% (DENV), 5.5% (cRGD-DENV/miR-375), 13.6% (cRGD-DENV-aPD-L1) and 22.7% (cRGD-DENV-aPD-L1/miR-375), respectively. The cRGD-DENV-aPD-L1/miR-375 exhibited higher early apoptotic induction rate compared with control group and DENV group. Moreover, the total apoptosis rate, including early and late apoptosis at five different treatments were about were 10.5%, 12.32%, 19.85%, 23.09%, 31.09%, respectively. It was demonstrated that the combination of aPD-L1 and miR-375 had significant statistical difference in apoptosis induction compared with control, DENV group and single aPD-L1/miR-375. ($p < 0.05$).

Studies have shown that miR-375 is significantly down-regulated in esophageal cancer and restoring miR-375 expression levels can significantly inhibit the proliferation, invasion, and metastasis of ESCC (esophageal squamous cell carcinoma); which indicates that miR-375 could be a candidate molecule for ESCC gene therapy[38, 39]. Research have shown that miR-375 overexpression may have impact on cell proliferation, migration and invasion by facilitating cell apoptosis[40]. To further investigate the possible mechanism of miR-375-mediated inhibition of cell proliferation and migration, firstly, we quantified the expression levels of miR-375 in five different treatments. Quantitative PCR results (Fig. 7B) showed that miR-375 expression levels in the cRGD-DENV/miR-375 and cRGD-DENV-aPD-L1/miR-375 groups were significantly increased compared with other groups. Next, YWHAZ, a predicted and identified target gene of miR-375, playing important roles in regulating cell apoptosis, invasion and migration[41] were selected to investigate the effect of engineered DENV on esophageal cancer cells. As shown in Fig. 7C-D, the YWHAZ protein expression level in cRGD-DENV/miR-375 group and cRGD-DENV-aPD-L1/miR-375 group was decreased greatly than control group, and the cRGD-DENV-aPD-L1/miR-375 group significantly inhibited YWHAZ expression. Therefore, cRGD-DENV-aPD-L1/miR-375 successfully delivered miR-375 to esophageal cancer cells to exert an inhibitory effect, affecting proliferation, migration and invasion of esophageal cancer cells by regulating YWHAZ.

In vivo targeting and anti-tumor effects of engineered DENV

cRGD-DENV mediated co-delivery of miR-375 and PD-L1 to the KYSE-150 cells had shown an ideal delivery effect *in vitro*. Subsequently, their delivery efficiency in vivo was evaluated by IVIS Lumina Ⅱ *In Vivo* Imaging System(PerkinElmer, USA). To demonstrate the tumor targeting ability and anti-tumor effects of engineered DENV *in vivo*, KYSE-150 serum-free cell suspension was injected subcutaneously into the armpit of the right limb of BALB/c nude mice. When the tumor volume reached 200 mm^3, they

were randomly divided into six groups with six mice in each group, treatment with saline, DENV, cRGD-DENV/miR-375, aPD-L1, cRGD-DENV-aPD-L1, cRGD-DENV-aPD-L1/miR-375, respectively. The schematic diagram of animal experiment was shown in Fig. 8A. Firstly, we investigated the targeting of the DIR labeled DENV and cRGD-DENV *in vivo.* After tail vein injection of DENV and cRGD-DENV, the biodistribution of injected DENV were monitored at different time points (Fig. 8B). At the earliest time point after injection (3 h), DENV and cRGD-DENV were rapidly distributed all over the body, with the difference that a large proportion of cRGD-DENV distributed in the tumor, which was indicative of the fast accumulation within the tumor area. Whereas DENV was located mainly in liver, suggesting that DENV uptake and retention took place primarily in the liver and other metabolic organs, with little accumulation in the tumor, similar to the results of previous studies that most intravenous EVs were more easily absorbed by the liver[42-44]. However, as time went on, striking differences were found between DENV and cRGD-DENV groups. A relatively intense fluorescence signal exclusively in the tumor area was detected after 6 h of injection cRGD-DENV and other parts of the body gradually decreased. Representative results were shown in Fig. 8B. Moreover, the relatively intense fluorescence signal still could be detected in the liver after 12h of injection DENV. In contrast, almost no signal was detected at the liver in the cRGD-DENV group, while the fluorescence signal only could be detected in tumor site (Fig. 8B), Fig. 8C-D showed the representative images in the cRGD-DENV group, indicating a rapid blood clearance by reticuloendothelial system. Taken together, these data suggested that cRGD-DENV could be served as an effective drug delivery carrier for targeting integrtin-expressing tumor.

Furthermore, the anti-tumor effect of engineered cRGD-DENV *in vivo* has been investigated. Compared with control group, mice injecting with cRGD-DENV-aPD-L1 and cRGD-DENV-aPD-L1/miR-375 had remarkable tumor inhibition over 25 days, noticeably, mice injected with cRGD-DENV-aPD-L1/miR-375 inhibited significantly tumor growth and decreased tumor volume (Fig. 8E-F). When cRGD-DENV-aPD-L1/miR-375 arrived at tumor site, the matrix metalloproteinase overexpressed in TME could cleave Gly-PLGLAG-Cys, aPD-L1 was released and interacted with PD-L1 receptors on tumor cells, which can enhance the anti-tumor effect of immune system *in vivo*. Consequential, miR-375 was delivered to tumor cells and then played a role in inhibiting tumor growth. Furthermore, during the treatment, no obvious weight loss was observed in each group (Fig. 8G), suggesting safety of this targeted delivery system based on DENV. These results further demonstrated the successful delivery of aPD-L1 *in vivo* and the favorable outcome of combination of immune and gene therapy.

Histological analysis

Caspase3 and caspase9 are commonly used indicators in apoptosis of various cells. Therefore, at the end of the investigation, the mice were sacrificed and tumor tissue sections were cut and performed apoptosis detection. As shown in Fig. 9, the expressions of caspase3 and caspase9 in cRGD-DENV-aPD-L1/miR-375 group were higher than other groups, indicating that the successful delivery of aPD-L1 *in vivo* and had an notable antitumor effects in tumor site. Studies have shown that treating with DC-TEX (tumor-derived exosome-pulsed dendritic cells) could increase $CD8^+$ T cells number and suppressed tumor growth in orthotopic HCC mice[45], while the inhibition of tumor growth caused by anti-SEMA4

blocking therapy in colorectal cancer tissue depended on the infiltrating $CD8^+$ T cells in tumor tissue[46]. Subsequently, we assessed the infiltration of lymphocytes by detecting the expression of CD3, CD4 and CD8 to determine how immune cell populations were affected by aPD-L1[47]. As we can see in Fig. 9, the groups of aPD-L1, cRGD-DENV-aPD-L1 and cRGD-DENV-aPD-L1/miR-375 had lymphocyte infiltration compared with control group, and the cRGD-DENV-aPD-L1/miR-375 group had the most lymphocyte infiltration, which indicated cRGD-DENV-aPD-L1/miR-375 could recruit more lymphocytes to combat tumor cells, thereby inhibiting tumor[48].

In vivo safety evaluation

In addition to treatment efficacy, toxicity is another critical consideration of an excellent delivery system for clinic use. For safety purpose, we evaluated the systematic toxicity of the different formulations in healthy BALB/c nude mice after intravenous injection. Compared with control group, no deaths and serious body weight loss were observed for the test groups. It is well-known that most intravenously injected nanoscale lipid vesicles were taken up and eliminated by mononuclear phagocyte system (MPS) [49]. Thus we further investigated the potential pathological lesions induced by the formulations on major organs. Blood biochemistry and hematology analysis were carried out to reveal any potential toxic effect of DENV on the treated mice. Different biochemistry parameters were tested including the liver function markers such as ALT, AST, the kidney function markers including CRE and BUN. As it could be seen in Tab. 2, all the above indexes levels remained the same as the untreated group, indicating that cRGD-DENV-aPD-L1/miR-375 had no obvious hepatic or renal toxicity within the dosage regimen. For the hematological assessment, white blood cell (WBC) counts were examined. All the above parameters of cRGD-DENV-aPD-L1/miR-375 group indicated no significant difference compared with control group (Tab. 2). Furthermore, as shown in Fig. 10, major tissues (including heart, liver, spleen, lung and kidney) had no obvious histopathological abnormalities or lesions in the cRGD-DENV-aPD-L1/miR-375 group. We further quantified the serum levels of IL-6, IL-1β and TNF-α, and no significance was observed among these groups (Fig. 11), which suggested that there was no evidence of inflammatory response caused by cRGD-DENV-aPD-L1/miR-375. All of these results showed that multiple dosage of cRGD-DENV-aPD-L1/miR-375 did not cause acute toxicity to the hematological system and major organs in mice.

Tab. 2 Serum levels of ALT, AST, CRE, BUN, WBC.

Group	Index	ALT(U/L)	AST(U/L)	CRE(μmol/L)	BUN(mmol/L)	WBC(10^9/L)
Control		3.02±1.49	9.88±5.76	4.88±1.23	2.96±1.65	6.54±44.94
DENV		3.72±4.78	2.68±0.94	4.97±2.45	2.09±0.29	6.21±5.27
cRGD-DENV/miR-375		2.94±1.93	5.14±3.54	5.00±5.64	2.24±0.65	8.26±10.20
aPD-L1		2.46±2.38	4.02±3.36	4.98±1.00	2.15±0.29	6.53±1.87
cRGD-DENV-aPD-L1		5.21±4.99	3.04±1.93	7.90±4.00	2.36±0.54	5.93±20.04
cRGD-DENV-aPD-L1/miR-375		2.54±1.22	3.65±0.52	6.67±2.05	3.16±0.62	6.33±2.72

Conclusions

In this study, we have developed successfully a combined strategy that exosome-like nanovesicle-based codelivery of miR-375 and aPD-L1 for enhancing tumor targeted therapy efficiency. More importantly, the exosome-like nanovesicles can be obtained in a high yield with less cost and time. Moreover, the exosome-like nanovesicle from *D. salina* with excellent biocompatibility was more likely to accumulate at tumor site than other nano-delivery system. In summary, the DENV-based delivery system combined gene therapy and immunotherapy is suitable for large-scale production, which may contribute to the establishment of a synergistic treatment with the potential to be translated into the clinics in the near future.

Materials And Methods

Materials

Fetal bovine serum was purchased from Wisent Biotechnology Co., Ltd. (Nanjing, China). Anti-PD-L1 (aPD-L1) was obtained from Invivogen (California, USA). The c(RGDyK) (cyclo(Arg-Gly-Asp-D-Tyr-Lys)) peptide and the Gly-PLGLAG-Cys polypeptide were synthesized by GL Biochem Co., Ltd. (Shanghai, China). 3-Maleimidobenzoic acid N-hydroxysuccinimide ester (MBS) and 2-Iminothiolane hydrochloride (Traut's Reagent) were purchased from Sigma-Aldrich (St. Louis, MO, USA). Annexin V-FITC Apoptosis Detection Kit was obtained from Sangon Biotech (Shanghai, China). Rabbit anti-caspase 9 antibody and anti-caspase 3 antibody were purchased from Boster Biological Engineering Co., Ltd. (Wuhan, China). Rabbit anti-CD3 antibody was obtained from Proteintech (Wuhan, China), anti-CD4 antibody and anti-CD8 antibody were purchased from Abcam (Shanghai, China).

Cell culture and animals

The human esophageal cancer cell lines KYSE-150 were purchased from the Cell Bank of the Chinese Academy of Sciences (Shanghai, China). KYSE-150 cells were cultured in Roswell Park Memorial

Institute-1640 medium (RPMI-1640) supplemented with 10% FBS and 1% penicillin-streptomycin at 37°C in 5% CO_2 incubators.

The female Balb/c nude mice (18-20g, 4-5 weeks old) were supplied by Nanjing Cavins Biotechnology Co., Ltd. and raised under 25 ± 1 °C with free access to food and water. All the animal experiments were carried out according to the guidelines approved by the ethics committee of Henan University of Science and Technology (Luoyang, China).

Isolation and purification of DENV

D. salina was cultured with PKS liquid medium (1.5 M NaCl, 10 mM KNO_3, 50 mM $NaHCO_3$, 5 mM $MgSO_4$·7H2O, 0.4 mM KH_2PO_4, 2 μM $FeCl_3$·$6H_2O$, 5 μM EDTA, 7 μM $MnCl_2$·$4H_2O$, 1 μM $CuCl_2$·$2H_2O$, 1μM $ZnCl_2$, 1 μM $CoCl_2$·$6H_2O$, 1 μM $(NH_4)Mo_7O_{24}$·$4H_2O$, 185 μM H_3BO_3, 0.2 mM $CaCl_2$) at the conditions (temperature 26 °C, light-dark ratio 14:10, light intensity 4000 Lux m^{-2} s^{-1}). Then the culture medium were collected and DENV was extracted using the ultracentrifugation method described below[36]. The specific steps are as follows: 1. Centrifuge the culture supernatant at 2,000 g at 4 °C for 20 min to remove the *D. salina* cells. 2. Take the supernatant from the previous step and centrifuge at 10,000 g for 30 min at 4 °C to remove cell debris. 3. Take the supernatant from the previous step and centrifuge at 100,000 ×g at 4 °C for 90 min. 4. Discard the supernatant and resuspend the DENV with PBS. Then DENV was quantified by BCA assay and stored at -80 °C after aliquoting.

Preparation and characterization of DENV and cRGD-DENV-aPD-L1/miR-375

Firstly, chemical coupling technology was used to prepare cRGD-DENV-PLGLAG by coupling of cRGD, Gly-PLGLAG-Cys peptide and DENV. The fluorescence co-localization method was used to determine the coupling efficiency. In brief, added DIO (0.5 μg/mL) to labeled DENV, and cRGD peptide were labeled by Cy5.5-NHS according to the manufacturer's instructions to obtain Cy5.5-cRGD, this process was achieved by the reaction of the amino group with NHS, and removed the unreacted excess dye through a purification column. Next, Cy5.5-cRGD (0.5 mg/mL) was mixed with an excess of Traut's reagent at room temperature for 30 min to generate sulfhydryl groups, at the same time, DIO-DENV were incubated with MBS (0.1 mg/mL) for 30 min to produce maleimide pendant groups on its outer membrane. After that, DENV were mixed with the thiolated cRGD and Gly-PLGLAG-Cys peptide solution for 1 h and obtained cRGD-DENV-PLGLAG. Then the cRGD-DENV-PLGLAG was mixed with Traut's reagent, meanwhile, the aPD-L1 incubated with MBS at room temperature for 30 min. Finally, cRGD-DENV-aPD-L1 was obtained by mixing aPD-L1 with thiolated cRGD-DENV-PLGLAG above, and then removed free unreacted substances by ultracentrifugation.

MiR-375 plasmid was loaded by a typical electroporation method. Briefly, cRGD-DENV or cRGD-DENV-aPD-L1 (0.5 mg/mL) and miR-375 plasmid (0.1 mg/mL) were mixed to 1 mL conductivity buffer, respectively. The miR-375 plasmid was loaded by electroporation under the conditions of 300 V, 250 μF.

After loading, they were centrifuged at 100,000g at 4 ° C for 90 min to remove unbound drugs and then resuspended in PBS.

Take the suspension of DENV and cRGD-DENV-aPD-L1/miR-375 on a copper grid, and leave them at room temperature for 5min, respectively. Drop 3% phosphotungstic acid solution on the copper mesh about 10μL, counterstain it for 5min. Bake with an incandescent lamp at 65 °C for about 15 min before taking pictures under the microscope and analyze the morphology of each sample by a TEM. The size distribution of the DENV and cRGD-DENV-aPD-L1/miR-375 were determined by Zetasizer Nano ZS instrument (Malvern, UK).

The sensitive properties of Gly-PLGLAG-Cys peptide to MMPs was confirmed by the release of aPD-L1 from cRGD-DENV-aPD-L1/miR-375 investigated in PBS containing or not MMPs, as well as cell experiment. For determination, the equilibrium dialysis method was applied to detect aPD-L1. cRGD-DENV-aPD-L1/miR-375 solution (2 mL) was filled into the dialysis bag followed by immersed in 50 mL PBS (pH 7.4, containing MMPs or not). Then the samples were shook for 8 h at 37 °C at 120 rpm. At predetermined time points, the samples were collected for quantitative analysis by HPLC system. Also, we studied whether pH (pH 7.4 and pH 6.5) had an effect on the release of aPD-L1 from cRGD-DENV-aPD-L1/miR-375, and the method was the same as above. For cell experiment, DIO and Cy5.5 fluorescent dyes were used to label DENV and aPD-L1, respectively. After preparing cRGD-DENV-aPD-L1/miR-375, it was added into KYSE-150 cells to detect the release of aPD-L1 via a confocal laser scanning microscope (ZEISS, Germany).

Cellular uptake

Briefly, DENV (0.5 mg/mL) was suspended in 100 μL of dye diluent and mixed with DIO (3 μL). After incubating at room temperature for 30 min, 1% BSA (1 mL) was added to stop the labeling reaction, and the ultracentrifugation method was used to re-isolate the labeled exosomes. When the confluence of KYSE-150 cells reached 50%, adding DAPI (10 μL) to the glass-bottom petri dish and incubating for 10 min, then washed with PBS. DIO-labeled DENV (5 μg) were added into KYSE-150 cells were observed during the period using a confocal laser scanning microscope with live cells work station to examine the cellular uptake of DIO-labeled DENV in different time point.

Cell proliferation experiment

In vitro cytotoxicity was measured by performing MTT assay on KYSE-150 cells. The cells (1×10^4/mL) were inoculated into a 96-well plate for 24 h; then incubated with different samples (Control, DENV, cRGD-DENV/miR-375, cRGD-DENV-aPD-L1, cRGD-DENV-aPD-L1/miR-375) for another 48 h. Thereafter, 10 μL MTT (5 mg/mL) was added to each well, and after incubating for another 4 h, DMSO (150 μL) was added to each well, and shook for 10 min to sufficiently melt the crystal. The absorbance of each well was determined at 490 nm on an enzyme-linked immunosorbent monitor, and the results were assayed.

Cell migration and invasion assay

The wound-healing assay was performed to study cell migration capacity as described previously[50]. KYSE-150 cells were seeded into 6-well plates, when they reached to 70%-80% confluence; a scratch in the cell monolayer was made, and then incubated with different samples (Control, DENV, cRGD-DENV/miR-375, cRGD-DENV-aPD-L1, cRGD-DENV-aPD-L1/miR-375). Finally, cells were recorded at 0, 12h, 24h, 48h.

Transwell experiment was used to investigate cellular invasion capacity *in vitro*. KYSE-150 cells were cultured in serum-free medium for 12-24 h to starve cells. After matrigel hydration in 24-well plate, serum-free medium was added to the upper chamber and cells (5×10^4) were seeded in each chamber. 10% serum-containing medium was added to the 24-well plate as an inducer. Added the experimental samples (Control, DENV, cRGD-DENV/miR-375, cRGD-DENV-aPD-L1, cRGD-DENV-aPD-L1/miR-375) after attaching, checked cells under the chamber at the nodes of 12 h, 24 h, 48 h, terminated experiment after detecting cells, carefully wipe the matrigel and cells in the upper chamber with a cotton swab, and then in the upper and lower chambers 4% paraformaldehyde (500 μL) was added for 30 min, finally, stained with 0.5% crystal violet. Three different fields were selected under an inverted microscope to calculate the number of cells invading and the invasion rate.

Flow cytometry

KYSE-150 cells (5×10^5) were seeded per well on a 6-well plate overnight, treating with PBS, DENV, cRGD-DENV/miR-375, cRGD-DENV-aPD-L1, cRGD-DENV-aPD-L1/miR-375, respectively. After 24 h, KYSE-150 cells were harvested and detected with the Annexin V-FITC Apoptosis Detection Kit according to the manufacture's protocol and the apoptosis ratio was analyzed by BD Accuri C6 flow cytometer and Modfit ™ software (BD Biosciences, Mountain View, CA, USA).

RT-PCR

After treating with different treatments (PBS, DENV, cRGD-DENV/miR-375, cRGD-DENV-aPD-L1, cRGD-DENV-aPD-L1/miR-375) for 48 h, total RNA was extracted with Trizol. Then, the RNA was reverse transcribed from the RTase according to the manufacturer's protocol. The reverse transcript primers used in this reaction system were listed in Tab. 1. Subsequently, the reverse transcript cDNA (1 μL) was added to the PCR system with forward and reverse primer, respectively. Finally, RNase-free water was used to supplement the reaction system. The reaction system was amplified at 95 °C for 15 s and at 60 °C for 1 min for 40 cycles. RNU6B was used as internal control, and the relative expression of miR-375 was evaluated based on the $2^{-\Delta\Delta CT}$ method.

Tab. 1 Gene specific primers sequences.

Name of primer	Forward primer (5’ to 3’)	Reverse primer (5’ to 3’)
RT-miR-375	CTCAACTGGTGTCGTGGAGTCGGC	AATTCAGTTGAGGGTTTGTG
miR-375	ACACTCCAGCTGGGGCGACGAGCCCCTCGCA	TGGTGTCGTGGAGTC
RNU6B	GCTTCGGCAGCACATATACTAAAAT	CGCTTCACGAATTTGCGTGTCAT

Western blot analysis

KYSE-150 cells were lysed with RIPA buffer comprising PMSF. Protein were mixed with 5 × loading buffer, and boiled for 5 min in water at 100 °C. Equal amounts of protein (10 μg) were separated by 10% SDS-PAGE and transferred to PVDF membranes, then blocked with 5% BSA in TBST for 1 h at room temperature. And the membrane was incubated with monoclonal antibodies YWHAZ (1:1,000) and GAPDH (1:1,000) overnight. After washing, the membrane was incubated with secondary antibody (1:2,000) for 2 h at room temperature. The bands were visualized by High-sig ECL western blotting substrate and analyzed on Tanon 5200 Chemiluminescence imaging system.

Evaluation and biodistribution of DENV *in vivo*

The esophageal cancer-bearing mice were constructed using the heterotopic transplantation method as reported previously with slight modification[51]. In brief, KYSE-150 serum-free cell suspension (1×10^7 cells/mL, 100 μL) was injected subcutaneously into armpit of right limb of Balb/c nude mice. After two weeks, recorded weight, tumor size of nude mice every three days until experiment end. Tumor volumes of the mice was calculated using the formula: tumor volume = (length × width^2)/2. When the tumor volume reached 200 mm^3, Balb/c nude mice were randomly divided into six groups with six mice in each group as follows: Group 1: Control (treated with saline), Group 2: DENV, Group 3: cRGD-DENV/miR-375, Group 4: aPD-L1, Group 5: cRGD-DENV-aPD-L1, Group 6: cRGD-DENV-aPD-L1/miR-375 (100μL) were respectively injected every three days for seven times.

For DENV biodistribution *in vivo*, DIR labeled DENV and cRGD-DENV (0.5mg/mL, 100 μL) were injected separately by tail vein, and the fluorescence images were captured after 3h via IVIS Lumina Ⅲ *In Vivo* Imaging System (PerkinElmer).

Histological analysis

With respect to biosafety, at the end of animal experiments, mice were sacrificed, and serum was obtained at the indicated times. To monitor the inflammatory response, serum TNF-α, IL-1β and IL-6 were detected by ELISA[52]. At the same time, pathological examinations of vital organs were performed to assess the biocompatibility of DENV *in vivo*. The major organs (including heart, liver, spleen, lung and kidney) of mice in different treatment groups were collected and fixed by paraformaldehyde, tissue dehydration, paraffin embedding, paraffin sectioning and H & E staining for histological evaluation.

Paraffin-embedded tissue sections were used to detect Caspase 3 and Caspase 9 expression, as well as infiltration of lymphocytes. Tissues sections with a 4 μm thicknesses were prepared and dewaxed with xylene I, II and Ⅲ for 15 min, respectively, and hydrate in gradient ethanol (100%, 95%, 85% and 75%) for an appropriate time, then washed with PBS for three times. After sections were dewaxed and rehydrated, antigen was repaired in boiling citric acid buffer (0.01 M, pH = 6) for 15 min. Then the universal SP kit mouse/rabbit streptavidin-biotin method detection system was used. For immunohistochemical analysis, sections were incubated at 4 °C overnight with anti-caspase 9, anti-caspase 3, anti-CD3, anti-CD4 and anti-CD8 antibody, respectively. Labeling was identified by application of a goat anti-rabbit IgG/HRP secondary antibody at 37 °C for 30 min. After washing with PBS, the sections were incubated with 3, 3'-diaminobenzidine (DAB), rinsed in water, counterstained with hematoxylin, differentiated with hydrochloric acid and ethanol. Finally, slides were observed using a ZEISS Axio Imager system.

Statistical analysis

Data were presented as the mean ± SD deviation of three technical replicates. Statistical analysis was performed using the two tailed t-test or one-way analysis of variance (ANOVA) to assess statistical significance between groups. $p < 0.05$ was considered statistically significant.

Declarations

Acknowledgments

Not applicable.

Authors' contributions

Gaofeng Liang and Mengxi Zhu designed this experiment and wrote the manuscript; Mengxi Zhu and Shan Li executed the experiment and data curation; Shuying Feng and Lina Hu supervised the experiment and gave some valuable advice; Haojie Wang validated it; Yingjie Yu and Shegan Gao edited the manuscript. All authors read and approved the final manuscript.

Funding

This work was financially supported by the National Natural Science Foundation of China (U1804193) and Innovation Scientists and Technicians Troop Construction Projects of Henan Province (CXTD2017071).

Availability of data and materials

All data generated or analyzed during this study are included in this manuscript.

Ethics approval and consent to participate

All animal experiments were approved by the Animal Ethics Committee of Henan University of Science and Technology.

Consent for publication

All authors are Consent for publication.

Competing interests

The authors declare that they have no competing interests.

Author details

[1] School of Basic Medical Sciences, Henan University of Science & Technology, Luoyang 471023, China;

[2] School of Basic Medical Sciences, Henan University of Chinese Medicine, No. 156, Jinshui East Road, Zhengzhou, Henan 450046, China;

[3] Henan Key Laboratory of Microbiome and Esophageal Cancer Prevention and Treatment; The First Affiliated Hospital of Henan University of Science and Technology, Luoyang 471023, China

References

[1] LIN Q, QU M, ZHOU B, et al. Exosome-like nanoplatform modified with targeting ligand improves anti-cancer and anti-inflammation effects of imperialine [J]. Journal of controlled release : official journal of the Controlled Release Society, 2019: 104-16.

[2] GONG C, TIAN J, WANG Z, et al. Functional exosome-mediated co-delivery of doxorubicin and hydrophobically modified microRNA 159 for triple-negative breast cancer therapy [J]. Journal of nanobiotechnology, 2019, 17(1): 93.

[3] KIM D, KOTHANDAN V, KIM H, et al. Noninvasive Assessment of Exosome Pharmacokinetics In Vivo: A Review [J]. Pharmaceutics, 2019, 11(12).

[4] CHEN R, XU X, QIAN Z, et al. The biological functions and clinical applications of exosomes in lung cancer [J]. Cellular and molecular life sciences : CMLS, 2019, 76(23): 4613-33.

[5] QI H, LIU C, LONG L, et al. Blood Exosomes Endowed with Magnetic and Targeting Properties for Cancer Therapy [J]. ACS nano, 2016, 10(3): 3323-33.

[6] HADLA M, PALAZZOLO S, CORONA G, et al. Exosomes increase the therapeutic index of doxorubicin in breast and ovarian cancer mouse models [J]. Nanomedicine (London, England), 2016, 11(18): 2431-41.

[7] MITTAL S, GUPTA P, CHALUVALLY-RAGHAVAN P, et al. Emerging Role of Extracellular Vesicles in Immune Regulation and Cancer Progression [J]. Cancers, 2020, 12(12).

[8] LIANG Y, DUAN L, LU J, et al. Engineering exosomes for targeted drug delivery [J]. Theranostics, 2021, 11(7): 3183-95.

[9] YOU J, KANG S, RHEE W. Isolation of cabbage exosome-like nanovesicles and investigation of their biological activities in human cells [J]. Bioactive materials, 2021, 6(12): 4321-32.

[10] TENG Y, XU F, ZHANG X, et al. Plant-derived exosomal microRNAs inhibit lung inflammation induced by exosomes SARS-CoV-2 Nsp12 [J]. Molecular therapy : the journal of the American Society of Gene Therapy, 2021.

[11] KIM M, AHN J, JEON H, et al. Development of a Dunaliella tertiolecta Strain with Increased Zeaxanthin Content Using Random Mutagenesis [J]. Marine drugs, 2017, 15(6).

[12] LUO S, ALIMUJIANG A, BALAMURUGAN S, et al. Physiological and molecular responses in halotolerant Dunaliella salina exposed to molybdenum disulfide nanoparticles [J]. Journal of hazardous materials, 2021, 404: 124014.

[13] LUDWIG B, TOMASSI S, DI MARO S, et al. The organometallic ferrocene exhibits amplified anti-tumor activity by targeted delivery via highly selective ligands to αvβ3, αvβ6, or α5β1 integrins [J]. Biomaterials, 2021, 271: 120754.

[14] JI X, HAN T, KANG N, et al. Preparation of RGD4C fused anti-TNFα nanobody and inhibitory activity on triple-negative breast cancer in vivo [J]. Life sciences, 2020, 260: 118274.

[15] BARI E, SERRA M, PAOLILLO M, et al. Silk Fibroin Nanoparticle Functionalization with Arg-Gly-Asp Cyclopentapeptide Promotes Active Targeting for Tumor Site-Specific Delivery [J]. Cancers, 2021, 13(5).

[16] SHI N, LI Y, ZHANG Y, et al. Intelligent "Peptide-Gathering Mechanical Arm" Tames Wild "Trojan-Horse" Peptides for the Controlled Delivery of Cancer Nanotherapeutics [J]. ACS applied materials & interfaces, 2017, 9(48): 41767-81.

[17] ZHANG D, HUANG Q. Encapsulation of Astragaloside with Matrix Metalloproteinase-2-Responsive Hyaluronic Acid End-Conjugated Polyamidoamine Dendrimers Improves Wound Healing in Diabetes [J]. Journal of biomedical nanotechnology, 2020, 16(8): 1229-40.

[18] MAO X, JIN F. The Exosome And Breast Cancer Cell Plasticity [J]. OncoTargets and therapy, 2019, 12: 9817-25.

[19] DESMOND B, DENNETT E, DANIELSON K. Circulating Extracellular Vesicle MicroRNA as Diagnostic Biomarkers in Early Colorectal Cancer-A Review [J]. Cancers, 2019, 12(1).

[20] RAPOSO G, STOORVOGEL W. Extracellular vesicles: exosomes, microvesicles, and friends [J]. The Journal of cell biology, 2013, 200(4): 373-83.

[21] XIE F, XU M, LU J, et al. The role of exosomal PD-L1 in tumor progression and immunotherapy [J]. Molecular cancer, 2019, 18(1): 146.

[22] DI GIOIA S, HOSSAIN M, CONESE M. Biological properties and therapeutic effects of plant-derived nanovesicles [J]. Open medicine (Warsaw, Poland), 2020, 15(1): 1096-122.

[23] MAN F, WANG J, LU R. Techniques and Applications of Animal- and Plant-Derived Exosome-Based Drug Delivery System [J]. Journal of biomedical nanotechnology, 2020, 16(11): 1543-69.

[24] MUNIR J, LEE M, RYU S. Exosomes in Food: Health Benefits and Clinical Relevance in Diseases [J]. Advances in nutrition (Bethesda, Md), 2020, 11(3): 687-96.

[25] GONABADI E, SAMADLOUIE H, SHAFAFI ZENOOZIAN M. Dunaliella salinaOptimization of culture conditions for enhanced productions in mixotrophic culture [J]. Preparative biochemistry & biotechnology, 2021: 1-9.

[26] SUI Y, HARVEY P. Dunaliella salinaEffect of Light Intensity and Wavelength on Biomass Growth and Protein and Amino Acid Composition of [J]. Foods (Basel, Switzerland), 2021, 10(5).

[27] ZHU Q, BAO J, LIU J, et al. High salinity acclimatization alleviated cadmium toxicity in Dunaliella salina: Transcriptomic and physiological evidence [J]. Aquatic toxicology (Amsterdam, Netherlands), 2020, 223: 105492.

[28] WALKER S, BUSATTO S, PHAM A, et al. Extracellular vesicle-based drug delivery systems for cancer treatment [J]. Theranostics, 2019, 9(26): 8001-17.

[29] SMYTH T, PETROVA K, PAYTON N, et al. Surface functionalization of exosomes using click chemistry [J]. Bioconjugate chemistry, 2014, 25(10): 1777-84.

[30] YANG J, WU S, HOU L, et al. Therapeutic Effects of Simultaneous Delivery of Nerve Growth Factor mRNA and Protein via Exosomes on Cerebral Ischemia [J]. Molecular therapy Nucleic acids, 2020, 21: 512-22.

[31] KIM G, KIM M, LEE Y, et al. Systemic delivery of microRNA-21 antisense oligonucleotides to the brain using T7-peptide decorated exosomes [J]. Journal of controlled release : official journal of the Controlled Release Society, 2020, 317: 273-81.

[32] FAN Z, CHANG Y, CUI C, et al. Near infrared fluorescent peptide nanoparticles for enhancing esophageal cancer therapeutic efficacy [J]. Nature communications, 2018, 9(1): 2605.

[33] LO W, LO S, CHEN S, et al. Molecular Imaging and Preclinical Studies of Radiolabeled Long-Term RGD Peptides in U-87 MG Tumor-Bearing Mice [J]. International journal of molecular sciences, 2021, 22(11).

[34] SHARMA M, TURAGA R, YUAN Y, et al. Simultaneously targeting cancer-associated fibroblasts and angiogenic vessel as a treatment for TNBC [J]. The Journal of experimental medicine, 2021, 218(4).

[35] TIAN T, ZHANG H, HE C, et al. Surface functionalized exosomes as targeted drug delivery vehicles for cerebral ischemia therapy [J]. Biomaterials, 2018, 150: 137-49.

[36] LIANG G, KAN S, ZHU Y, et al. Engineered exosome-mediated delivery of functionally active miR-26a and its enhanced suppression effect in HepG2 cells [J]. International journal of nanomedicine, 2018, 13: 585-99.

[37] GU G, XIA H, HU Q, et al. PEG-co-PCL nanoparticles modified with MMP-2/9 activatable low molecular weight protamine for enhanced targeted glioblastoma therapy [J]. Biomaterials, 2013, 34(1): 196-208.

[38] HU C, LV L, PENG J, et al. MicroRNA-375 suppresses esophageal cancer cell growth and invasion by repressing metadherin expression [J]. Oncology letters, 2017, 13(6): 4769-75.

[39] ISOZAKI Y, HOSHINO I, AKUTSU Y, et al. Usefulness of microRNA-375 as a prognostic and therapeutic tool in esophageal squamous cell carcinoma [J]. International journal of oncology, 2015, 46(3): 1059-66.

[40] HE Z, LI W, ZHENG T, et al. Human umbilical cord mesenchymal stem cells-derived exosomes deliver microRNA-375 to downregulate ENAH and thus retard esophageal squamous cell carcinoma progression [J]. Journal of experimental & clinical cancer research : CR, 2020, 39(1): 140.

[41] ZHAO J, ZHAO Q, HU H, et al. The ASH1-miR-375-YWHAZ Signaling Axis Regulates Tumor Properties in Hepatocellular Carcinoma [J]. Molecular therapy Nucleic acids, 2018, 11: 538-53.

[42] YAO C, WANG P, LI X, et al. Near-Infrared-Triggered Azobenzene-Liposome/Upconversion Nanoparticle Hybrid Vesicles for Remotely Controlled Drug Delivery to Overcome Cancer Multidrug Resistance [J]. Advanced materials (Deerfield Beach, Fla), 2016, 28(42): 9341-8.

[43] HAO Y, LI W, ZHOU X, et al. Microneedles-Based Transdermal Drug Delivery Systems: A Review [J]. Journal of biomedical nanotechnology, 2017, 13(12): 1581-97.

[44] FU Y, XIONG S. Tagged extracellular vesicles with the RBD of the viral spike protein for delivery of antiviral agents against SARS-COV-2 infection [J]. Journal of controlled release : official journal of the Controlled Release Society, 2021, 335: 584-95.

[45] RAO Q, ZUO B, LU Z, et al. Tumor-derived exosomes elicit tumor suppression in murine hepatocellular carcinoma models and humans in vitro [J]. Hepatology (Baltimore, Md), 2016, 64(2): 456-72.

[46] EVANS E, JONASON A, BUSSLER H, et al. Antibody Blockade of Semaphorin 4D Promotes Immune Infiltration into Tumor and Enhances Response to Other Immunomodulatory Therapies [J]. Cancer immunology research, 2015, 3(6): 689-701.

[47] XIE Y, DOUGAN M, JAILKHANI N, et al. Nanobody-based CAR T cells that target the tumor microenvironment inhibit the growth of solid tumors in immunocompetent mice [J]. Proceedings of the National Academy of Sciences of the United States of America, 2019, 116(16): 7624-31.

[48] TUMEH P, HARVIEW C, YEARLEY J, et al. PD-1 blockade induces responses by inhibiting adaptive immune resistance [J]. Nature, 2014, 515(7528): 568-71.

[49] SUK J, XU Q, KIM N, et al. PEGylation as a strategy for improving nanoparticle-based drug and gene delivery [J]. Advanced drug delivery reviews, 2016, 99: 28-51.

[50] YU F, LIANG M, HUANG Y, et al. Hypoxic tumor-derived exosomal miR-31-5p promotes lung adenocarcinoma metastasis by negatively regulating SATB2-reversed EMT and activating MEK/ERK signaling [J]. Journal of experimental & clinical cancer research : CR, 2021, 40(1): 179.

[51] LIANG G, ZHU Y, ALI D, et al. Engineered exosomes for targeted co-delivery of miR-21 inhibitor and chemotherapeutics to reverse drug resistance in colon cancer [J]. Journal of nanobiotechnology, 2020, 18(1): 10.

[52] ZHANG N, SONG Y, HUANG Z, et al. Monocyte mimics improve mesenchymal stem cell-derived extracellular vesicle homing in a mouse MI/RI model [J]. Biomaterials, 2020, 255: 120168.

Figures

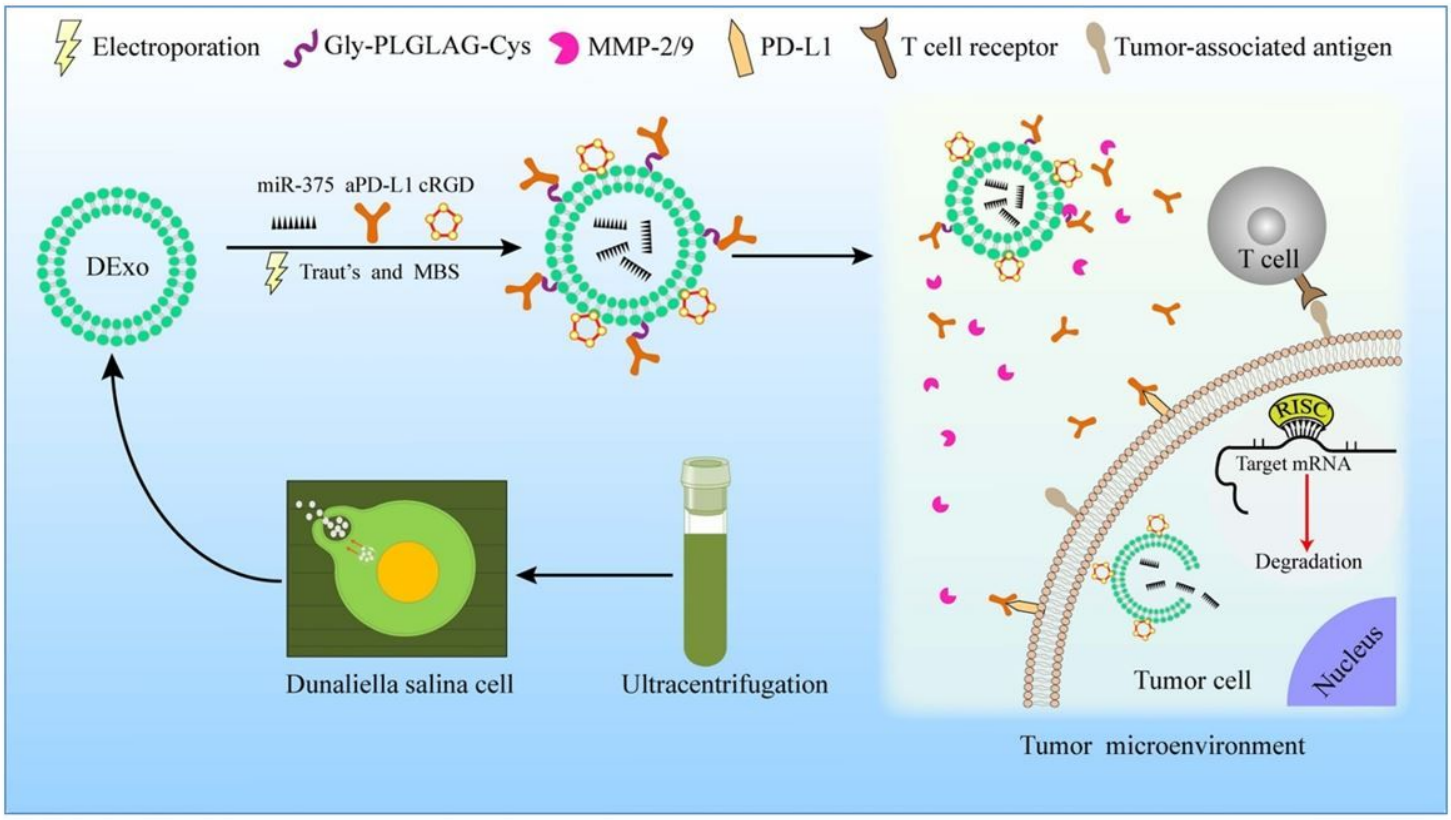

Figure 1

Schematic design of targeted drug delivery system based on DENV and their regulation strategy. The targeted drug delivery system accumulated in the tumor site due to the cRGD peptide, which exhibits high affinity to integrin αvβ3. The unregulated MMP-2/9 in the TME cleaves the MMP-2/9-sensitive substrate peptide (Gly-PLGLAG-Cys) and release aPD-L1, binding to the PD-L1 receptor on tumor cells in order to enhance the killing effect of T lymphocytes to tumor cells. Then the cRGD-DENV carrying miR-375 can be taken up by tumor cells for intracellular deep delivery miR-375, playing a therapeutic role at the gene level.

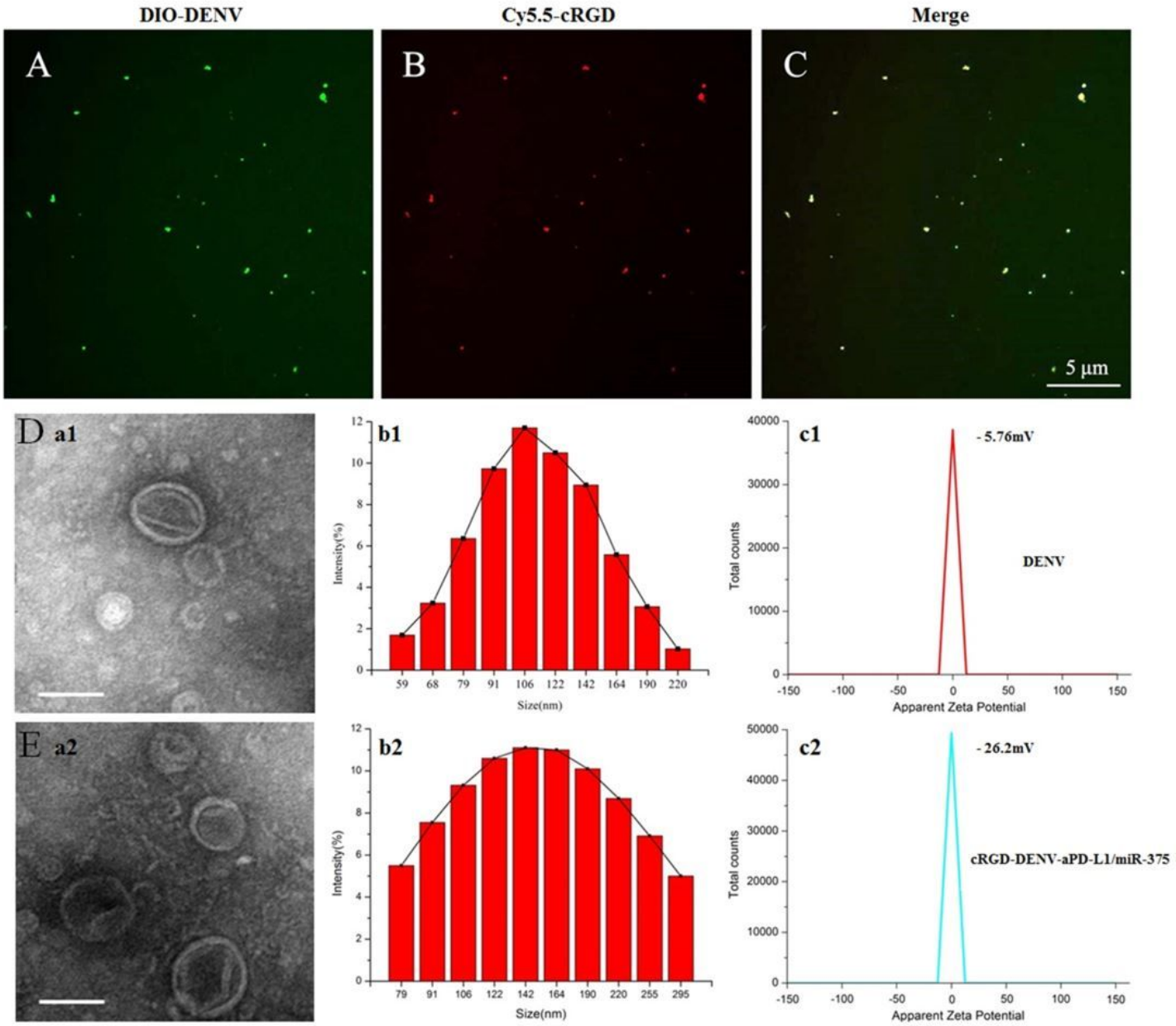

Figure 2

Characterization of DENV and cRGD-DENV-aPD-L1/miR-375. (A-C) Fluorescent overlay of DENV loaded with cRGD peptide. Scale bar = 5 μm. (D) The morphology (a1), size (b1), and Zeta potential (c1) of DENV. (E) The morphology (a2), size (b2), and Zeta potential (c2) of cRGD-DENV-aPD-L1/miR-375. Scale bar = 100 nm.

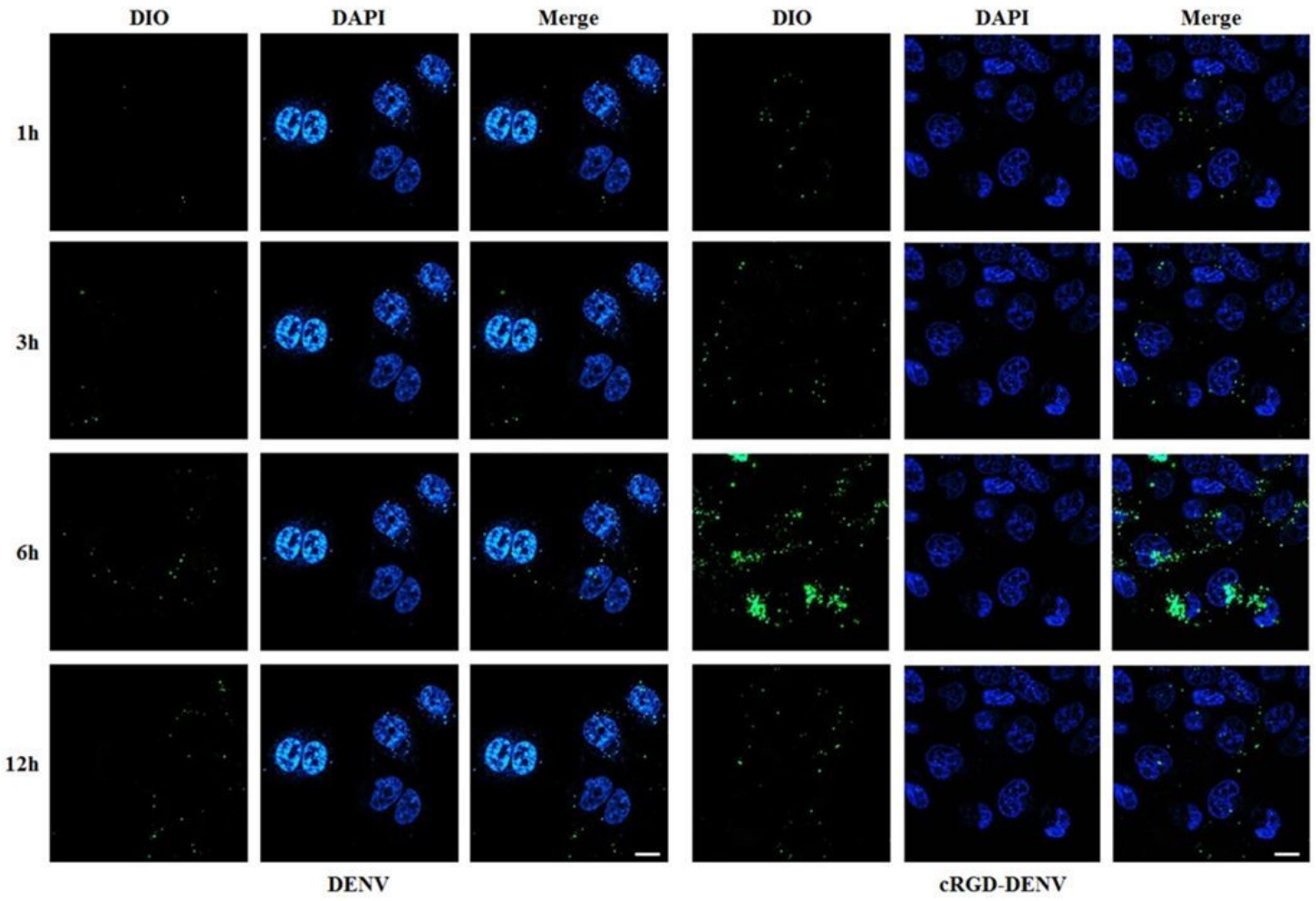

Figure 3

Observation of DIO labeled DENV entering esophageal cancer cells under CLSM in 12h. Scale bar = 5 μm.

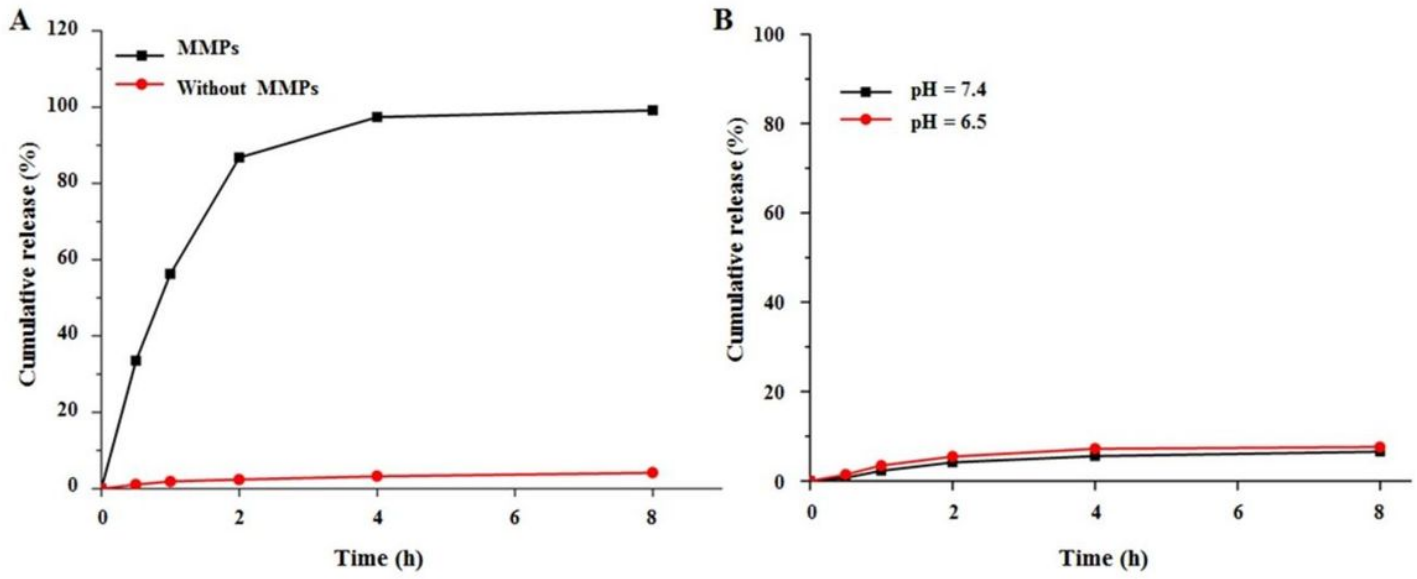

Figure 4

Assay of aPD-L1 release in PBS. (A) Release of aPD-L1 from cRGD-DENV-aPD-L1/miR-375 determined in the medium of PBS containing MMPs or not. (B) In vitro release of aPD-L1 from cRGD-DENV-aPD-L1/miR-375 in PBS (pH = 7.4 and pH = 6.5).

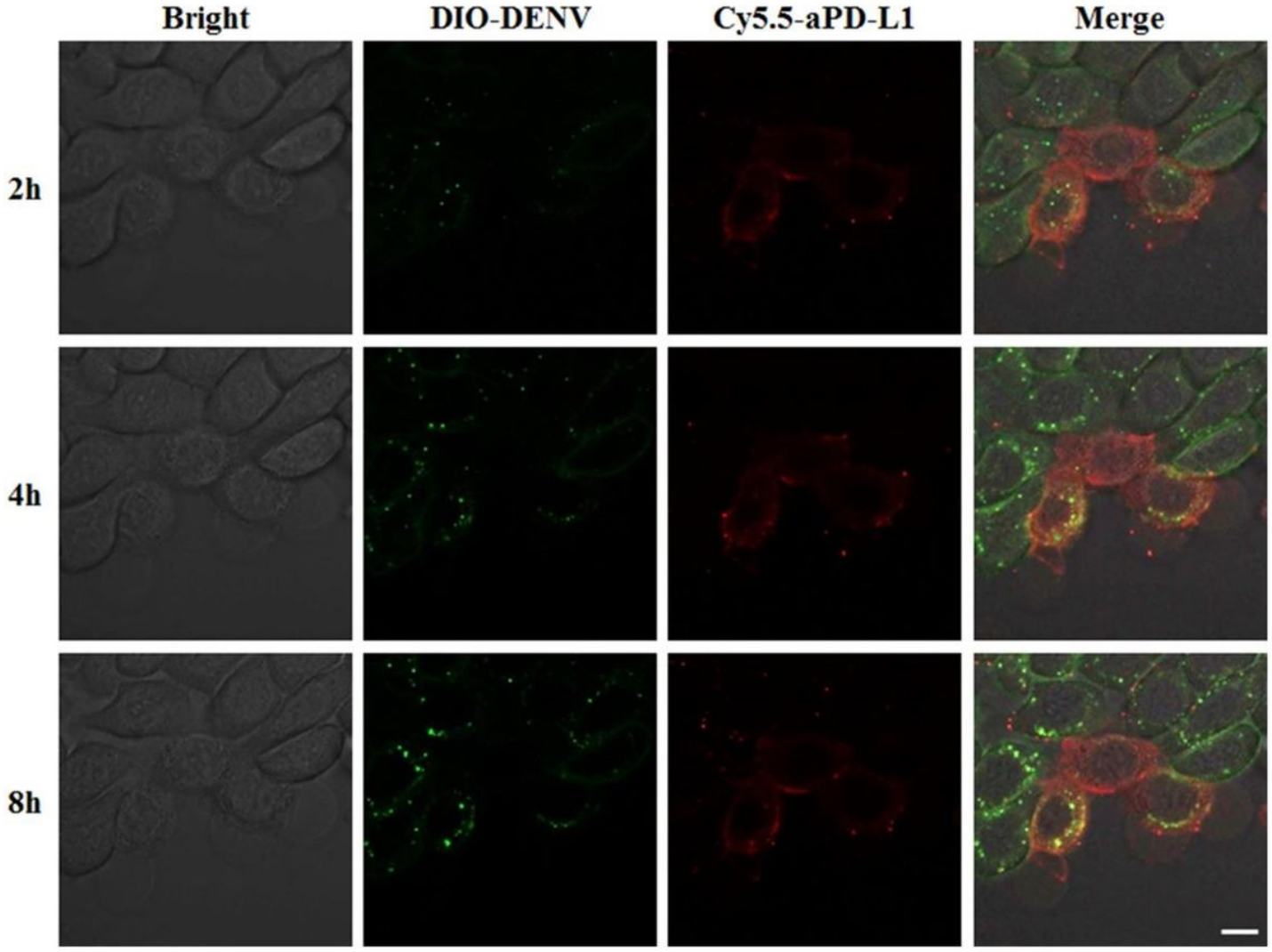

Figure 5

Evaluation of the sensitivity of cRGD-DENV-aPD-L1/miR-375 to MMPs in esophageal cells. Scale bar = 5 μm.

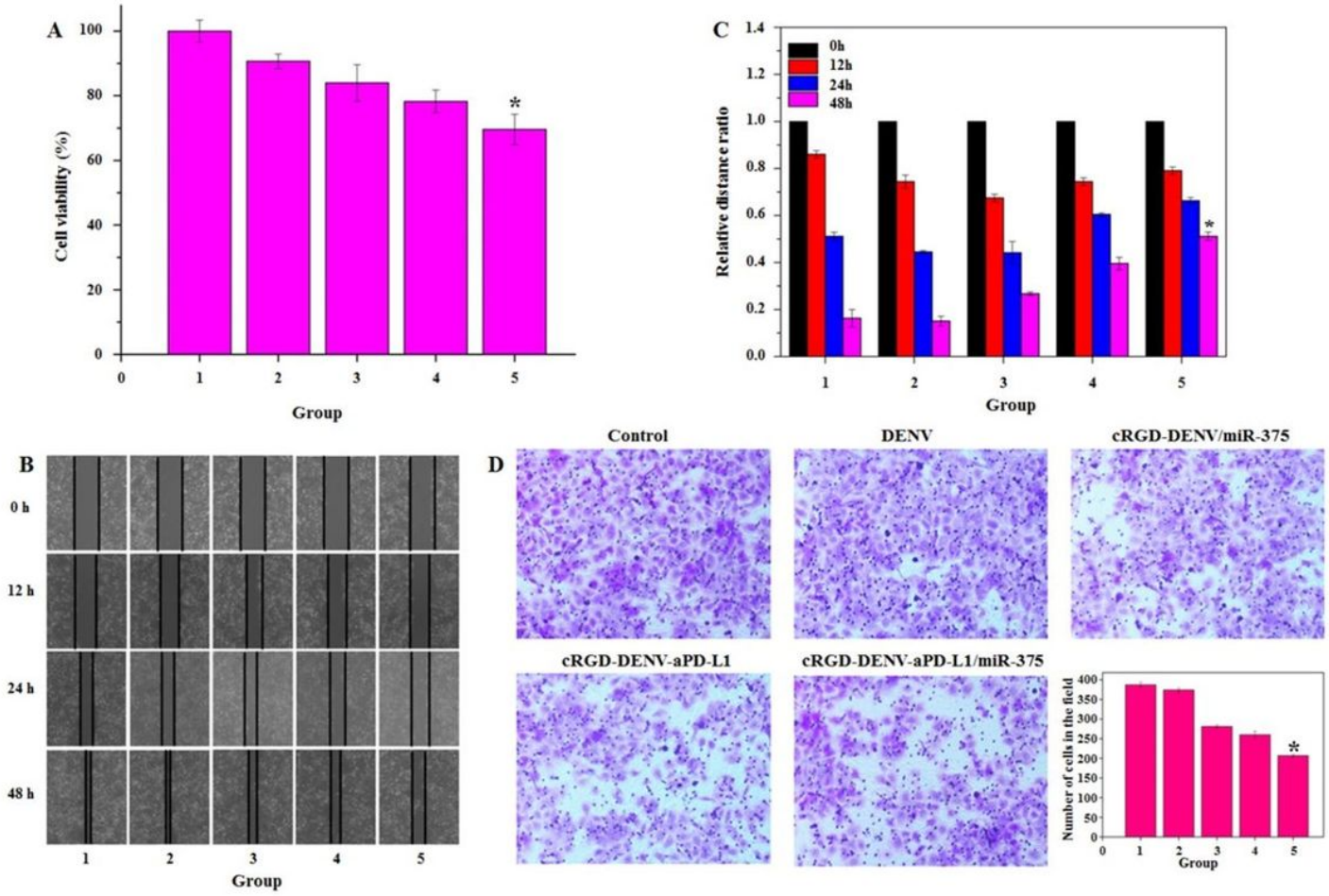

Figure 6

The effect of engineered DENV on proliferation, migration and invasion of esophageal cancer cells. (A) The cytotoxicity of engineered DENV (Group1: Control, Group2: DENV, Group3: cRGD-DENV/miR-375, Group4: cRGD-DENV-aPD-L1, Group5: cRGD-DENV-aPD-L1/miR-375). (B) Cell wound healing experiment treated with different samples in KYSE-150 cells at 0 h, 12h, 24 h and 48h. (C) Quantitative analysis based on wound-healing results in (C). (D) Transwell experiment treated with different samples in KYSE-150 cells at 48 h. (*$p < 0.05$, when compared with control).

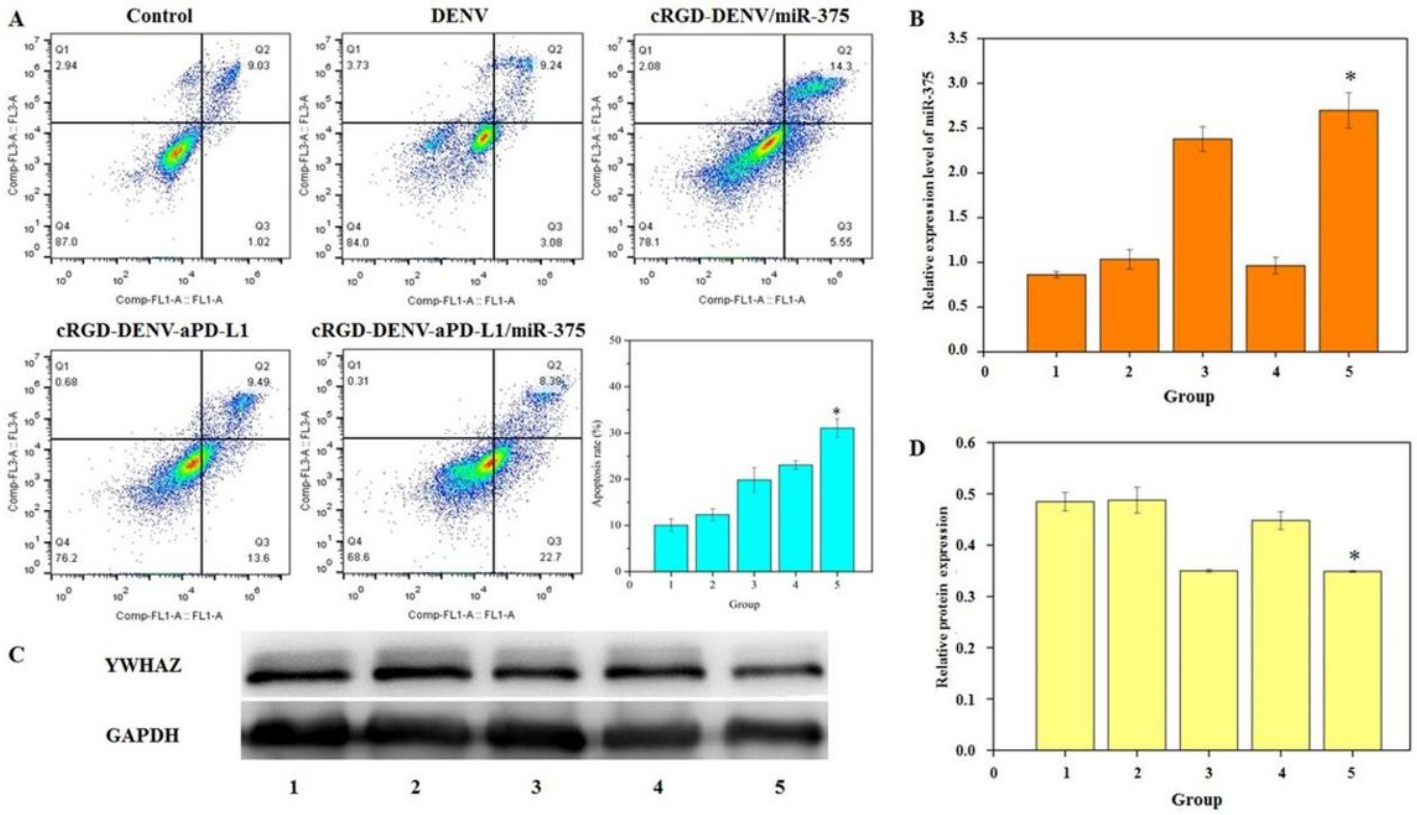

Figure 7

Flow cytometry, PCR and Western blot analysis of KYSE-150 cells after treating with PBS, DENV, cRGD-DENV/miR-375, cRGD-DENV-aPD-L1 and cRGD-DENV-aPD-L1/miR-375. (A) Cell apoptosis of KYSE-150 cell treated with different samples within 48h. (B) The expression of miR-375 in KYSE-150 cell. (C) Western blot analysis of YWHAZ expression in KYSE-150 cell. (D) Quantitative analysis based on YWHAZ expression in (C). (Group1: Control, Group2: DENV, Group3: cRGD-DENV/miR-375, Group4: cRGD-DENV-aPD-L1, Group5: cRGD-DENV-aPD-L1/miR-375. *p < 0.05, when compared with control).

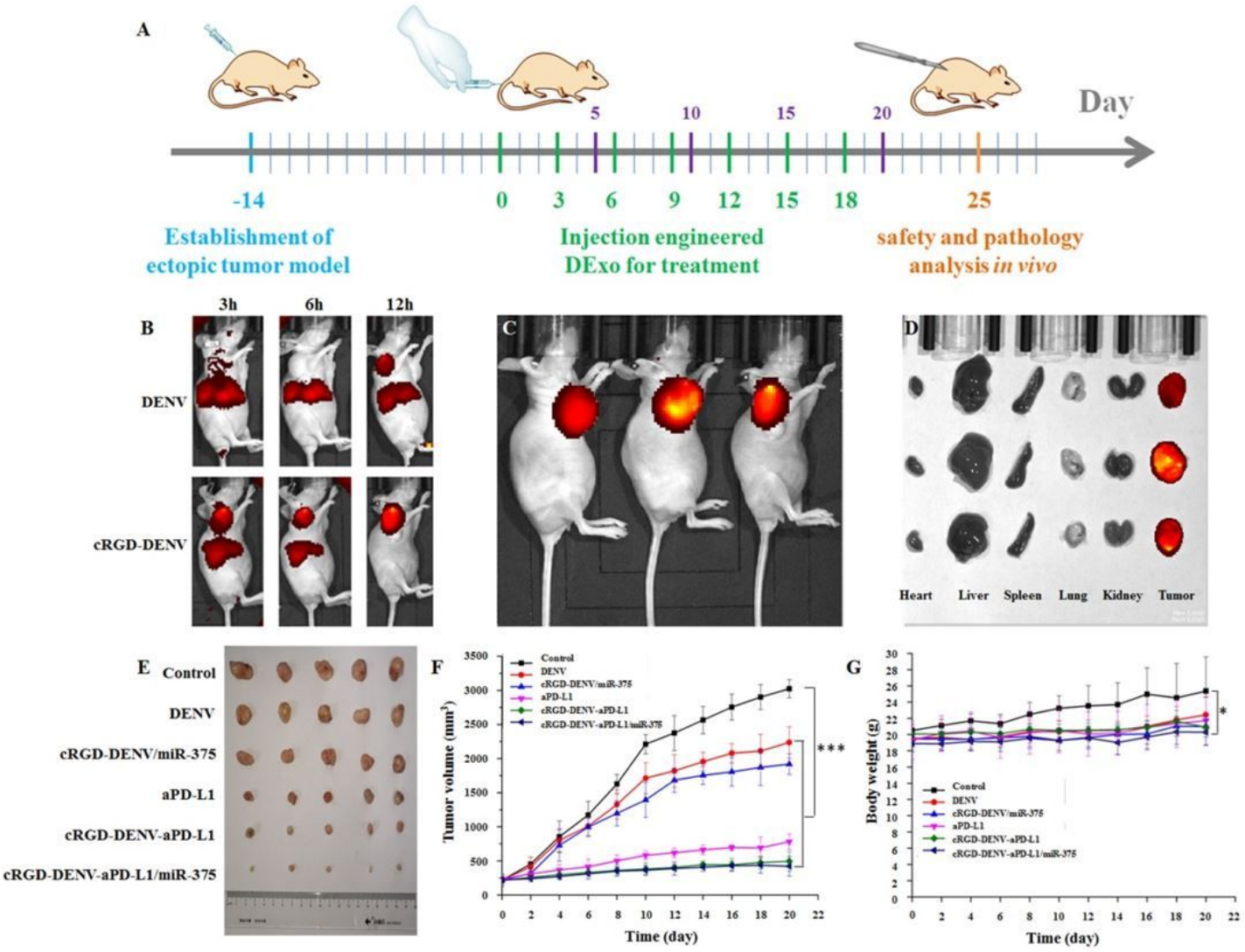

Figure 8

Anti-tumor evaluation in vivo. (A) Animal experiment plan. (B) The NIRF imaging of mice at different times after administration DENV and cRGD-DENV. (C) The NIRF imaging of mice at 12 h after administration cRGD-DENV. (D) The NIRF imaging of main organs at 12 h after administration cRGD-DENV. (E-F) Tumor sizes and volumes of nude mice after treated with saline (Control), DENV, cRGD-DENV/miR-375, aPD-L1, cRGD-DENV-aPD-L1, cRGD-DENV-aPD-L1/miR-375 by tail vein injection. (G) Body weight changes of each group during treatment. (*p < 0.05, **p < 0.01, ***p < 0.01 when compared with control).

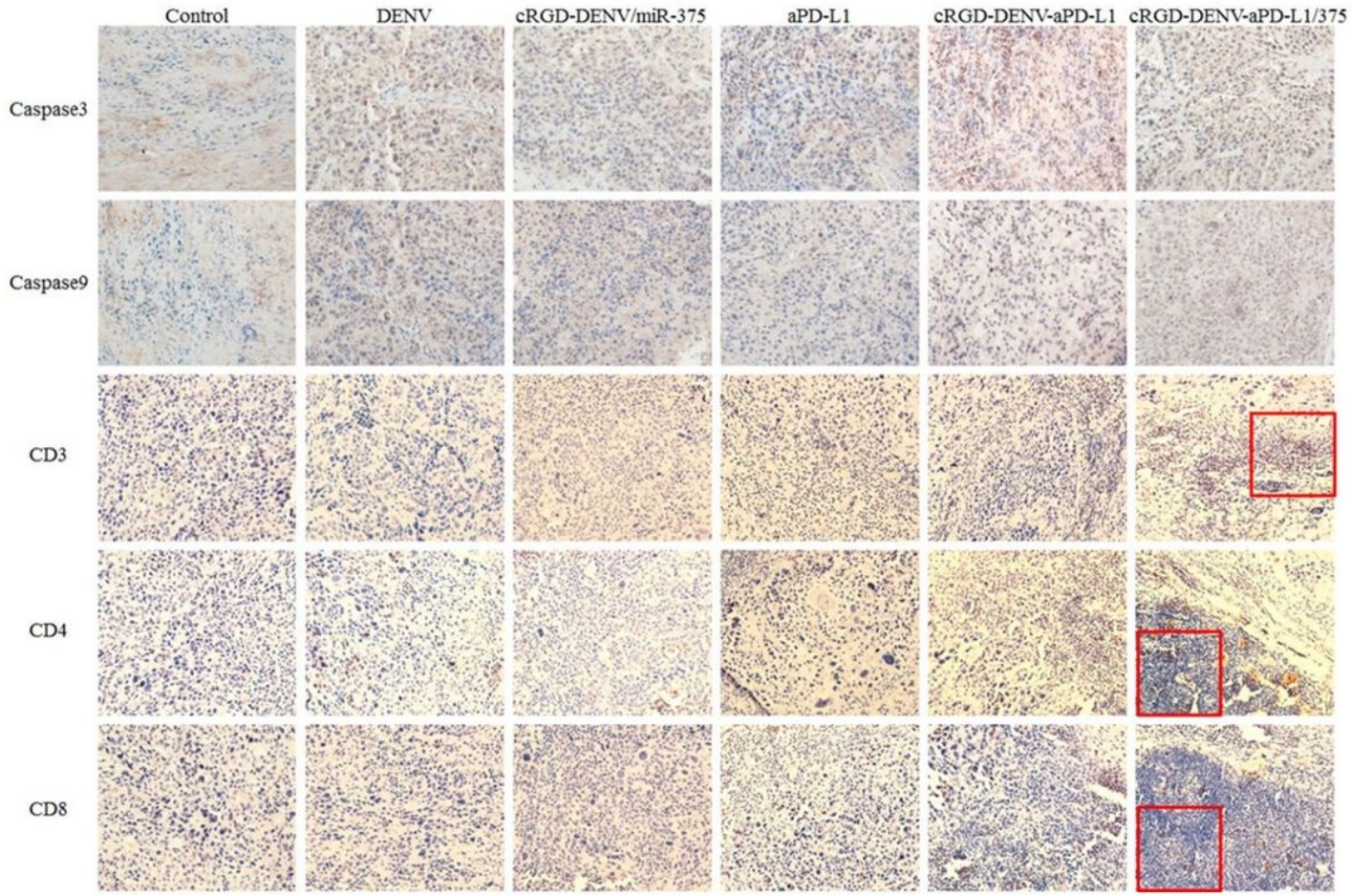

Figure 9

Immunohistochemical analyses of caspase 3, caspase 9, CD3, CD4 and CD8 for tumor tissues (20×).

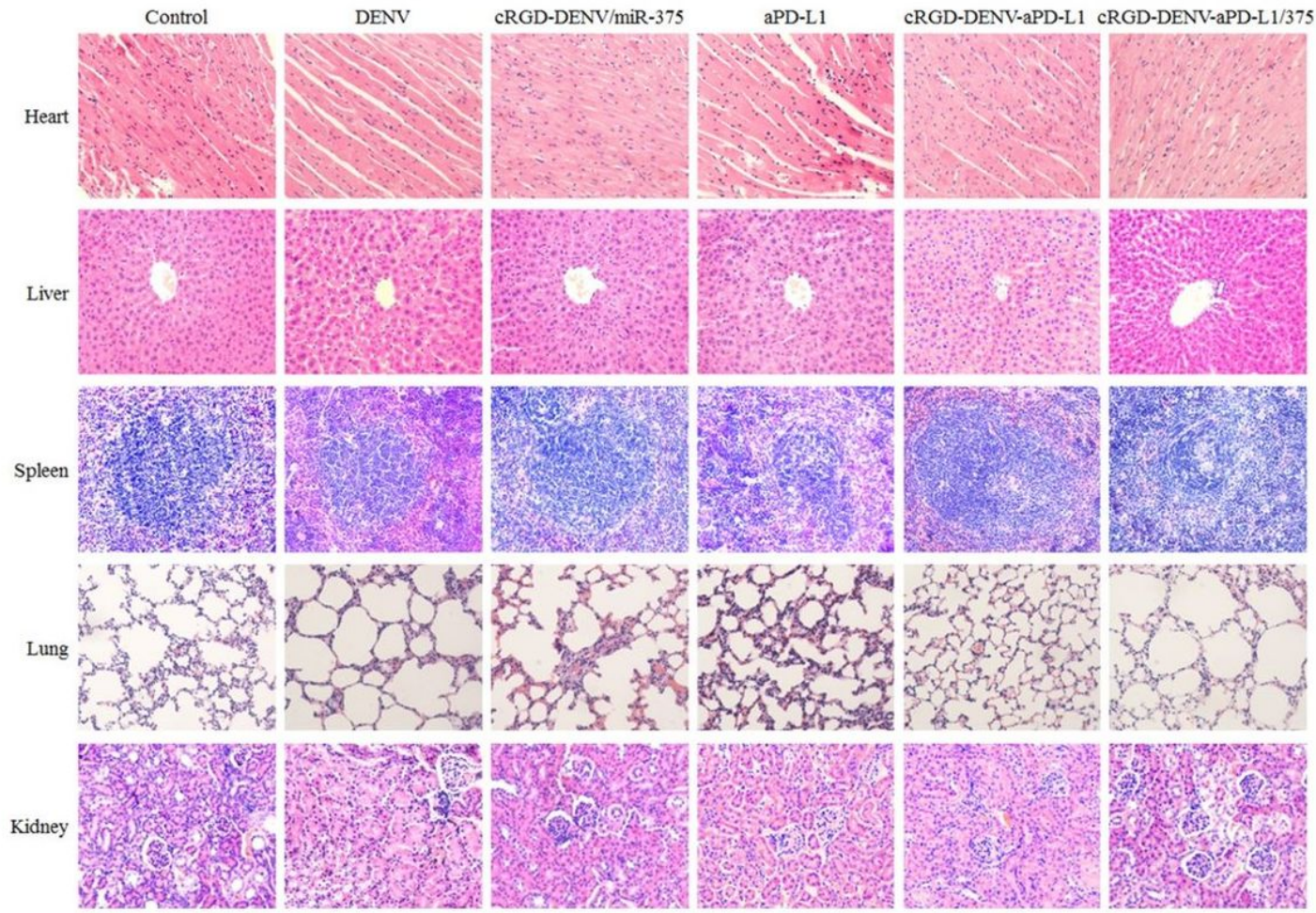

Figure 10

HE staining of major organs after treated with saline (Control), DENV, cRGD-DENV/miR-375, aPD-L1, cRGD-DENV-aPD-L1, cRGD-DENV-aPD-L1/miR-375.

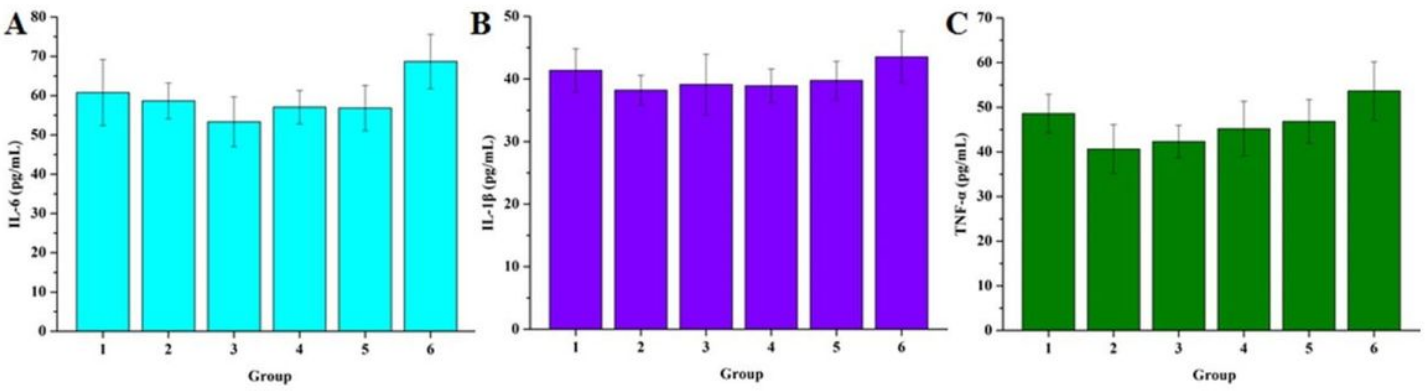

Figure 11

Serum levels of IL-6(A), IL-1β(B) and TNF-α(C).(Group1: Control, Group2: DENV, Group3: cRGD-DENV/miR-375, Group4: aPD-L1, Group5:cRGD-DENV-aPD-L1, Group6:cRGD-DENV-aPD-L1/miR-375)

Supplementary Files

This is a list of supplementary files associated with this preprint. Click to download.

- Graphicalabstract.docx